Noname manuscript No.
(will be inserted by the editor)

Optimum Cuts in Graphs by General Fuzzy Connectedness with Local Band Constraints

Caio de Moraes Braz · Paulo A.V. Miranda · Krzysztof Chris Ciesielski · Fábio A.M. Cappabianco

Received: date / Accepted: date

Abstract The goal of this work is to describe an efficient algorithm for finding a binary segmentation of an image such that: the indicated object satisfies a novel high-level prior, called Local Band, LB, constraint; the returned segmentation is optimal, with respect to an appropriate graph cut measure, among all segmentations satisfying the given LB constraint. The new algorithm has two stages: expanding the number of edges of a standard edge-weighted graph of an image; applying to this new weighted graph an algorithm known as an Oriented Image Foresting Transform, OIFT. In our theoretical investigation, we prove that OIFT algorithm belongs to a class of General Fuzzy Connectedness algorithms and so, has several good theoretical properties, like robustness for seed placement. The extension of the graph constructed in the first stage ensures, as we prove, that the resulted object indeed satisfies the given LB constraint. We also notice that this graph construction is flexible enough to allow combining it with other high-level constraints. Finally, we experimentally demonstrate that the LB constraint gives competitive results as compared to Geodesic Star Convexity, Boundary Band, and Hedgehog Shape Prior, all implemented within OIFT framework and applied to various scenarios involving natural and medical images.

Keywords boundary band constraint · hedgehog shape prior · image foresting transform · graph-cut segmentation

Thanks to CNPq (313554/2018-8, 486988/2013-9, FINEP 1266/13), FAPESP (2014/12236-1,2016/21591-5), Coordenação de Aperfeiçoamento de Pessoal de Nível Superior - Brasil (CAPES) - Finance Code 001, and NAP eScience - PRP - USP for funding.

C.M. Braz and P.A.V. Miranda
University of São Paulo, Institute of Mathematics and Statistics,
CEP 05508-090, São Paulo, SP, Brazil,
Tel.: +55-11-3091-5502
E-mail: {caiobraz, pmiranda}@ime.usp.br

K.C. Ciesielski
Department of Mathematics, West Virginia University, Morgantown, USA
E-mail: Krzysztof.Ciesielski@mail.wvu.edu

F.A.M. Cappabianco
Instituto de Ciência e Tecnologia,
São José dos Campos, SP, Brazil,
E-mail: cappabianco@unifesp.br

1 Introduction

Image segmentation is one of the most fundamental and challenging problems in image processing and computer vision. In many scenarios, the high-level, application-domain specific knowledge of the user is often required in the segmentation process because of the presence of heterogeneous backgrounds, objects with ill-defined borders, field inhomogeneity, noise, artifacts, partial volume effects, and their interplay [23]. It may be thought of as consisting of two related processes – object recognition and delineation [14]. Recognition is the task of determining an object's approximate whereabouts in the image. Delineation completes segmentation by defining the exact spatial extent of that object. In this work, we are interested in solving the delineation problem by fast methods to efficiently deal with large amounts of data, but which must also be versatile enough to support the inclusion of high-level constraints from prior object knowledge.

The segmentation problem can be interpreted as a graph partition problem subject to hard constraints, such as seed pixels selected in the image domain for object recognition, by modelling neighborhood relations of

picture elements from digital images. Examples of seed-based methods are watershed [10], random walks [16], fuzzy connectedness [6], graph cuts (GC) [2], grow cut [22], minimum barrier distance [9], and image foresting transform (IFT) [13,7]. Some methods, including the min-cut/max-flow algorithm, can provide global optimal solutions according to a graph-cut measure in graphs and can be described in a unified manner according to a common framework, which we refer to as Generalized Graph Cut (GGC) [4]. (See also [5].)

Oriented Image Foresting Transform (OIFT) [28] and *Oriented Relative Fuzzy Connectedness* (ORFC) [1] are extensions of some GGC methods for directed weighted graphs, which have lower computational complexity compared to the min-cut/max-flow algorithm [2]. Also, as we will show, OIFT belongs to a class of General Fuzzy Connectedness algorithms described in [8]. OIFT is a flexible method, which has been extended to support the processing of global object properties, such as connectedness [25,24], shape constraints [27,11], boundary polarity [26,1], and hierarchical constraints [20]. These high-level priors are potentially useful for object segmentation, allowing the customization of the segmentation to a given target object. Shape constraints can be used to eliminate undesirable intricate forms, improving the segmentation of objects with more regular contour. Some shape constraints demand more sophisticated algorithms, such as the *Boundary Band constraint* (BB) [11]. The OIFT with the BB constraint allows the segmentation to follow a pre-established template of shapes, with variances within a range of permitted deformations around an arbitrary scale, while other approaches handle scale inefficiently based on brute force, by computing the graph cut for each level of a gaussian pyramid [15].

In this work, we propose a novel shape constraint, named *Local Band constraint* (LB), to be used for object segmentation in the Generalized GC framework and which, in its limit case, is strongly related to the Boundary Band constraint [11]. The LB constraint demonstrates competitive results with higher accuracy when compared to BB, Hedgehog [19,18], and Geodesic Star Convexity [17] in various scenarios. It can also be easily combined with other high-level priors already supported by OIFT, considerably advancing the targeted segmentation [21].

The next section gives the required background on image graphs and GGC. In Sections 3 and 4 we show, respectively, that OIFT can be seen as belonging to the Generalized Graph Cut and the General Fuzzy Connectedness frameworks. This is the new material, that has not been presented in the conference version of the paper [12]. The proposed Local Band constraint is presented in Section 5. In Section 6, we experimentally evaluate LB, comparing it to previous graph-based works on shape constraints. Our conclusions are stated in Section 7.

2 Background

An image can be interpreted as a directed graph (digraph) $G = \langle \mathcal{N}, \mathcal{A} \rangle$ whose nodes/vertices are the image pixels in its image domain $\mathcal{N} \subset \mathbb{Z}^n$ and whose arcs/edges, elements of $\mathcal{A}$, are the ordered pixel pairs $\langle s, t \rangle$ of vertices that are adjacent, that is, spatially close (e.g., 4-neighborhood, or 8-neighborhood, in the case of 2D images). We write $t \in \mathcal{A}(s)$ or $\langle s, t \rangle \in \mathcal{A}$ to indicate that t is adjacent to s. We will usually assume also that our image graph G is edge-weighted, that is, that each arc $\langle s, t \rangle \in \mathcal{A}$ has a fixed weight $\omega(s, t) \in [-\infty, \infty]$ (often $\omega(s, t) = \|\mathcal{I}(t) - \mathcal{I}(s)\|$ for an image with values given by $\mathcal{I}(t)$). An edge weighted digraph will be denoted as $G = \langle \mathcal{N}, \mathcal{A}, \omega \rangle$. A digraph G is symmetric if, for all $\langle s, t \rangle \in \mathcal{A}$, the pair $\langle t, s \rangle$ is also an arc of G. Note that in symmetric graphs we can have $\omega(s, t) \neq \omega(t, s)$. In this work, all considered graphs are symmetric and connected.

A *path (in G)* of length $\ell \geq 0$ is any sequence $p_v = \langle v_0, \ldots, v_\ell \rangle$ of vertices, with *terminus* $v = v_\ell$, such that $\langle v_j, v_{j+1} \rangle \in \mathcal{A}$ for any $j < \ell$; it is *from* $\mathcal{S} \subset \mathcal{N}$ *to* $v \in \mathcal{N}$ when $v_0 \in \mathcal{S}$ and $v_\ell = v$; if $\langle v, w \rangle \in \mathcal{A}$, then $p_v \hat{} w$ denotes the path $\langle v_0, \ldots, v_\ell, w \rangle$. Let Π_G be the family of all paths in G and consider a path-cost function $\psi \colon \Pi_G \to [-\infty, \infty]$.

Image segmentation can be formulated as a graph partition problem subject to hard constraints. In the case of binary segmentation (object/background), we consider two non-empty disjoint seed sets $\mathcal{S}_1$ and $\mathcal{S}_0$ containing pixels selected inside the object $\mathcal{O}$ and in its exterior, respectively. A label, $L(t) = 1$ for all $t \in \mathcal{S}_1$ and $L(t) = 0$ for all $t \in \mathcal{S}_0$, is propagated to all unlabeled pixels during the execution of seed-based segmentation algorithms, see e.g. [28]. For a label map $L \colon \mathcal{N} \to \{0, 1\}$ the object $\mathcal{O}$ identified with it is defined as the set $L^{-1}(1)$, where $L^{-1}(i) := \{t \in \mathcal{N} \colon L(t) = i\}$.

In what follows, the key tool for finding optimized label maps L is the OIFT Algorithm 1, which comes from [26,28]. The OIFT will be a part of our novel algorithm. The map L it returns constitutes a global optimum solution that maximizes the following graph-cut measure

$$\varepsilon_{\min}(L) := \min\{\omega(s, t) \colon \langle s, t \rangle \in \mathcal{A} \ \&\ L(s) > L(t)\} \quad (1)$$

subject to the seed constraints [26,28]:

Proposition 1 [Mansilla, Miranda 2013] *Let $G = \langle \mathcal{N}, \mathcal{A}, \omega \rangle$ be a symmetric edge weighted image digraph. Let L be a segmentation returned by Algorithm 1 applied to G and non-empty disjoint seed sets $\mathcal{S}_1$ and $\mathcal{S}_0$. Then L satisfies the seed constraints and maximizes the energy $\varepsilon_{\min}$, given by (1), among all segmentations satisfying these constraints.*

Notice that in line 12 of Algorithm 1 the weight $\omega(t,s)$ of the reversed parallel arc $\langle t,s \rangle$ is used (rather than that of chosen $\langle s,t \rangle \in \mathcal{A}$). That is why a symmetric digraph is required. The OIFT Algorithm 1 can also be adapted for multi-object segmentation by computing a related variant in a hierarchical layered digraph [20].

In the next two sections, we will show that OIFT belongs to two general algorithmic frameworks: GGC and GFC.

Algorithm 1 – Segmentation Algorithm OIFT

Input: Symmetric edge weighted image digraph $\langle \mathcal{N}, \mathcal{A}, \omega \rangle$ and non-empty disjoint seed sets $\mathcal{S}_1$ and $\mathcal{S}_0$.
Output: The label map $L \colon \mathcal{N} \to \{0,1\}$.
Auxiliary: Priority queue Q, variable *tmp*, and an array of status $S \colon \mathcal{N} \to \{0,1\}$, where $S(t) = 1$ for processed nodes and $S(t) = 0$ for unprocessed nodes. The value $V(t)$ represents a potential penalty that a change of $L(t)$ would contribute to $\varepsilon_{\min}(L)$.

1. **For each** $t \in \mathcal{N}$, **do**
2. Set $S(t) \leftarrow 0$ and $V(t) \leftarrow \infty$;
3. **If** $t \in \mathcal{S}_0$, **then**
4. $V(t) \leftarrow -\infty$, $L(t) \leftarrow 0$, and insert t in Q;
5. **If** $t \in \mathcal{S}_1$ **then**
6. $V(t) \leftarrow -\infty$, $L(t) \leftarrow 1$, and insert t in Q.
7. **While** $Q \neq \emptyset$ **do**
8. Remove s from Q such that $V(s)$ is minimum.
9. Set $S(s) \leftarrow 1$.
10. **For each** $(s,t) \in \mathcal{A}$ such that $S(t) = 0$ **do**
11. **If** $L(s) = 1$, **then** $tmp \leftarrow \omega(s,t)$.
12. **Else** $tmp \leftarrow \omega(t,s)$;
13. **If** $tmp < V(t)$, **then**
14. Set $V(t) \leftarrow tmp$ and $L(t) \leftarrow L(s)$.
15. **If** $t \notin Q$, **then** insert t in Q.
16. Return L.

3 OIFT as a Generalized Graph Cut algorithm

The biggest difference between the above version of OIFT and the algorithms in the GGC framework [4] is that in the former case we *maximize* the energy function, while in the latter case we *minimize* its analog. To represent OIFT as a minimization problem it is enough to reverse in it all inequalities, exchange terms "∞" with "$-\infty$" and "minimum" with "maximum," and replace the weight function $\omega(s,t)$ with a function[1] $\bar{\omega}(s,t) := e^{-\omega(s,t)}$. Specifically, we represent OIFT as OIFT* Algorithm 2, for which we have the following result.

Proposition 2 *OIFT Algorithm 1 applied to $\langle \mathcal{N}, \mathcal{A}, \omega \rangle$ and the seed sets $\mathcal{S}_1$ and $\mathcal{S}_0$ returns the label map L if, and only if, L is returned by OIFT* Algorithm 2 applied to the same graph, seed sets, and the weight functions w_0 and w_1 (on $\mathcal{A}$) defined as $w_1(s,t) = \bar{\omega}(s,t)$ and $w_0(s,t) = \bar{\omega}(t,s)$.*

An easy proof of Proposition 2 is left to the reader. (We introduce in OIFT* the functions w_i and an explicit path map $\pi[]$ to help in our analysis in the next section.)

Algorithm 2 – OIFT* Algorithm

Input: Image graph $\langle \mathcal{N}, \mathcal{A} \rangle$, weight maps w_0 and w_1, seed sets $\mathcal{S}_0$ and $\mathcal{S}_1$.
Output: The label map $L \colon \mathcal{N} \to \{0,1\}$ and an array $\pi[]$ such that if $S(t) = 1$, then $\pi[t]$ is a path from $\mathcal{S}_{L(t)}$ to t.
Auxiliary: Priority queue Q, variable *tmp*, the cost function $V \colon \mathcal{N} \to [-\infty, \infty]$, and a status function $S \colon \mathcal{N} \to \{0,1\}$, where $S(t) = 1$ for processed nodes and $S(t) = 0$ for unprocessed nodes.

1. **For each** $t \in \mathcal{N}$, **do**
2. Set $S(t) \leftarrow 0$, $V(t) \leftarrow -\infty$, and $\pi[t] \leftarrow \langle t \rangle$;
3. **If** $t \in \mathcal{S}_0$, **then**
4. $V(t) \leftarrow \infty$, $L(t) \leftarrow 0$, and insert t in Q;
5. **If** $t \in \mathcal{S}_1$ **then**
6. $V(t) \leftarrow \infty$, $L(t) \leftarrow 1$, and insert t in Q.
7. **While** $Q \neq \emptyset$ **do**
8. Remove s from Q with $V(s) \geq V(t)$ for all $t \in Q$;
9. Set $S(s) \leftarrow 1$;
10. **For each** $\langle s,t \rangle \in \mathcal{A}$ such that $S(t) = 0$ **do**
11. $tmp \leftarrow w_{L(s)}(s,t)$;
12. **If** $tmp > V(t)$ **then**
13. Set $V(t) \leftarrow tmp$, $\pi[t] \leftarrow \pi[s]\hat{}\,t$ and $L(t) \leftarrow L(s)$.
14. **If** $t \notin Q$ **then** insert t in Q.

Now, let

$$X_L := \{\langle s,t \rangle \in \mathcal{A} \colon L(s) > L(t)\}$$

be the (standard) graph cut associated with the partition $\langle L^{-1}(1), L^{-1}(0) \rangle$ and define the functional[2] $F_L \colon \mathcal{A} \to [0,\infty)$ by putting, for every $\langle s,t \rangle \in \mathcal{A}$,

$$F_L(s,t) := \begin{cases} e^{-\omega(s,t)} & \text{for } \langle s,t \rangle \in X_L, \\ 0 & \text{otherwise.} \end{cases}$$

Then, OIFT* Algorithm 2 minimizes the energy

$$\|F_L\|_\infty := \max\{F_L(s,t) \colon \langle s,t \rangle \in \mathcal{A}\},$$

[1] In fact, we can use $h(\omega(s,t))$ in place of $e^{-\omega(s,t)}$ when h is any strictly decreasing function from $\mathbb{R}$ into $[0,\infty)$.

[2] Shortly, $F_L := \bar{\omega} \cdot \chi_{X_L}$, where $\chi_{X_L} \colon \mathcal{A} \to \{0,1\}$ is the characteristic function of X_L.

that is, the L_∞ norm of the functional F_L. This puts OIFT*, which is equivalent to OIFT, within the framework of Generalized Graph Cut, GGC, see e.g. [4]. (Recall, that the usual graph cut minimization, associated with the max-flow/min-cut theorem, is defined as L_1 norm of the functional F_L, defined as $\|F_L\|_1 := \sum_{\langle s,t\rangle\in\mathcal{A}} F_L(s,t)$.)

4 OIFT within General Fuzzy Connectedness framework

In the previous section we have seen that OIFT Algorithm 1 belongs to the GGC framework. Here, we will argue that it can be also viewed as belonging to a class of General Fuzzy Connectedness, GFC, algorithms [8]. This will allow us to deduce that OIFT has the properties that all algorithms in GFC are known to have.

In what follows, for a fixed digraph $\langle\mathcal{N},\mathcal{A}\rangle$, weight maps w_0 and w_1, and the seed sets $\mathcal{S}_0$ and $\mathcal{S}_1$, define the path costs:

$$\psi_{\min}(\langle v_0,\ldots,v_\ell\rangle) := \min_{1\le j\le\ell} w_{L(v_0)}(v_{j-1},v_j)$$

$$\psi_{\text{last}}(\langle v_0,\ldots,v_\ell\rangle) := w_{L(v_0)}(v_{\ell-1},v_\ell)$$

for $\ell > 0$ and

$$\psi_{\text{last}}(\langle v_0\rangle) := \psi_{\min}(\langle v_0\rangle) := \begin{cases}\infty & \text{for } v_0\in\mathcal{S}_0\cup\mathcal{S}_1,\\ -\infty & \text{otherwise.}\end{cases}$$

The map $\psi_{\min}$ is the standard FC cost, while ψ_{last}, explicitly defined in [26] (using symbols $f_{i,\omega}$ and $f_{o,\omega}$), is naturally associated with OIFT. (Compare also [7].)

Algorithm 3 – MOFS* Algorithm

INPUT: Image graph $\langle\mathcal{N},\mathcal{A}\rangle$, affinities w_0 and w_1, seed sets $\mathcal{S}_0$ and $\mathcal{S}_1$.
OUTPUT: The label map $L\colon\mathcal{N}\to\{0,1\}$ and an array $\pi[\,]$ such that if $S(t)=1$, then $\pi[t]$ is a path from $\mathcal{S}_{L(t)}$ to t.
AUXILIARY: Priority queue Q, variable *tmp*, the cost function $V\colon\mathcal{N}\to[-\infty,\infty]$, and a status function $S\colon\mathcal{N}\to\{0,1\}$, where $S(t)=1$ for processed nodes and $S(t)=0$ for unprocessed nodes.

1. **For each** $t\in\mathcal{N}$, **do**
2. | *Set* $S(t)\leftarrow 0$, $V(t)\leftarrow-\infty$, *and* $\pi[t]\leftarrow\langle t\rangle$;
3. | **If** $t\in\mathcal{S}_0$, **then**
4. | | $V(t)\leftarrow\infty$, $L(t)\leftarrow 0$, *and insert* t *in* Q;
5. | **If** $t\in\mathcal{S}_1$ **then**
6. | | $V(t)\leftarrow\infty$, $L(t)\leftarrow 1$, *and insert* t *in* Q.
7. **While** $Q\neq\emptyset$ **do**
8. | *Remove from* Q *an* s *in* $M=\{u\in Q\colon\psi_{\min}(\pi[u])=\max_{t\in Q}\psi_{\min}(\pi[t])\}$ *such that* $V(s)\ge V(u)$ *for all* $u\in M$;
9. | *Set* $S(s)\leftarrow 1$;
10. | **For each** $\langle s,t\rangle\in\mathcal{A}$ *such that* $S(t)=0$ **do**
11. | | $tmp\leftarrow w_{L(s)}(s,t)$;
12. | | **If** $\psi_{\min}(\pi[s]\hat{}\,t)>\psi_{\min}(\pi[t])$ *or* $[\psi_{\min}(\pi[s]\hat{}\,t)=\psi_{\min}(\pi[t])$ *and* $tmp>V(t)]$ **then**
13. | | | *Set* $V(t)\leftarrow tmp$, $\pi[t]\leftarrow\pi[s]\hat{}\,t$ *and* $L(t)\leftarrow L(s)$;
14. | | | **If** $t\notin Q$ **then** *insert* t *in* Q.

To place OIFT in the GFC framework, we will first represent OIFT* of Algorithm 2 as the MOFS* Algorithm 3, which is a version of MOFS algorithm from [8]. The key result here is the following theorem, which is considerably less clear than Proposition 2, since the conditions in lines 8 and 12 of the algorithms have different forms.

Theorem 3 (OIFT* in GFC format) *Any output of OIFT* Algorithm 2 is identical to that of MOFS* Algorithm 3. In particular, the algorithms MOFS* and OIFT are equivalent.*

We will postpone the proof of Theorem 3 to the end of this section.

Notice, that although OIFT* Algorithm 2 has a format of the MOFS algorithm from the GFC framework, it is not precisely of this format. The first difference is that the main GFC algorithm MOFS, when it removes a vertex s from the queue, does no have the secondary condition "$V(s)\ge V(u)$ for all $u\in M$" as we have in line 8. But this just means, that in MOFS* we are just a bit more precise, when making such choice.

The bigger difference is that MOFS allows some overlap of the object and background. Specifically, they overlap on the tie zone set TZ defined as the set of all $v\in\mathcal{N}$ for which MOFS, whose output is unique, produces the paths of the same strength from the object and the background. The issue of how to deal with the set TZ is discussed in details in [8]. In particular, if $w_0(s,t)\neq w_1(u,v)$ for all edges $\langle s,t\rangle$ and $\langle u,v\rangle$, then TZ is empty and the object returned by MOFS* (or OIFT*) is identical to that of MOFS output. Other solutions of the "overlapping problem" are also discussed in [8]. The reader should be warned, however, that a simple minded removal of TZ from the MOSF object (with overlap) may create a set with vertices that are not connected, within the object, to the seeds.

4.1 Proof of Theorem 3

First notice that, during the execution of OIFT* Algorithm 2, for any $u\in Q$ either u is a seed or $\pi[u]=\pi[w]\hat{}\,u$ for some $w\in\mathcal{N}$ with $S(w)=1$.

To prove the theorem, it is enough to show that during the execution of OIFT* Algorithm 2, the condition from line 8 holds, if and only if, the condition from line 8 of MOFS* Algorithm 3 holds. Similarly, for the conditions from line 12.

To see this, we will prove that, at any time of the execution of OIFT* Algorithm 2 past the line 6 of the code, the following holds for every $u, v \in \mathcal{N}$:

(i) if $S(u) = 1$ and $S(v) = 0$, then $\psi_{\min}(\pi[u]) \geq \psi_{\min}(\pi[v])$;
(ii) if $S(u) = S(v) = 0$ and $V(u) \geq V(v)$, then $\psi_{\min}(\pi[u]) \geq \psi_{\min}(\pi[v])$.

Clearly this holds directly after the execution of line 6. Thus, it is enough to show that these properties are preserved by any consecutive single execution of the while loop, that is, of lines 8-14.

So, fix $u, v \in \mathcal{N}$ for which we will be showing preservation of (i) and (ii). If u is a seed, then after the initialization we have $\psi_{\min}(\pi[u]) = V(u) = \infty$, so (i) and (ii) hold. So, we will assume that u is not a seed. Next, assume that during our execution of lines 8-14 we have taken s from Q.

To see that (ii) is preserved, assume that, after the execution of lines 8-14, we have $S(u) = S(v) = 0$. During the execution, the values of either $V(v)$ or $\pi[v]$ can change only in line 13, when $v = t$ for t chosen in line 10 and, during the execution of line 12, we have $w_{L(s)}(s, v) = w_{L(s)}(s, t) = tmp > V(t)$. Hence, the execution of line 13 results with $V(v) = V(t)$ becoming $w_{L(s)}(s, v)$ and $\pi[v] = \pi[t]$ becoming $\pi[s]\hat{}v = \pi[s]\hat{}t$ so that

$$\psi_{\min}(\pi[v]) = \min\{\psi_{\min}(\pi[s]), w_{L(s)}(s, v)\}.$$

The similar analysis holds when either of the values $V(u)$ or $\pi[u]$ are changed during the execution of lines 8-14.

Now, consider 4 cases:

- If none of the values $V(v)$, $\pi[v]$, $V(u)$, or $\pi[u]$ changes during the execution of lines 8-14, then clearly (ii) is preserved.
- If, during the execution, we applied the changes in line 13 to both u and v, then $V(u) \geq V(v)$ implies that $w_{L(s)}(s, u) \geq w_{L(s)}(s, v)$ and so,

$$\begin{aligned}\psi_{\min}(\pi[u]) &= \min\{\psi_{\min}(\pi[s]), w_{L(s)}(s, u)\} \\ &\geq \min\{\psi_{\min}(\pi[s]), w_{L(s)}(s, v)\} = \psi_{\min}(\pi[v])\end{aligned}$$

  giving desired (ii).
- If, during the execution, we applied the changes in line 13 only to u, then $\psi_{\min}(\pi[u]) = \min\{\psi_{\min}(\pi[s]), w_{L(s)}(s, u)\} \geq \psi_{\min}(\pi[s]) \geq \psi_{\min}(\pi[v])$, where the last inequality is implied by $V(s) \geq V(v)$, ensured by the choice of s from Q, and the recursive assumption (ii). Thus, indeed (ii) is preserved.
- Finally, if, during the execution, we applied the changes in line 13 only to v, then $V_{\text{old}}(u) = V_{\text{new}}(u) \geq V_{\text{new}}(v) = w_{L(s)}(s, v)$. Also, since u is not a seed, we have $\pi[u] = \pi[w]\hat{}u$ for some $w \in \mathcal{N}$ with $S(w) = 1$. By (i), used just before we have taken s from Q, we have $\psi_{\min}(\pi[w]) \geq \psi_{\min}(\pi[s])$. Therefore,

$$\begin{aligned}\psi_{\min}(\pi[u]) &= \min\{\psi_{\min}(\pi[w]), V(u)\} \\ &\geq \min\{\psi_{\min}(\pi[s]), w_{L(s)}(s, v)\} \\ &= \psi_{\min}(\pi[v])\end{aligned}$$

  finishing the proof of preservation of (ii).

Next, we will prove preservation of (i). So, assume that after the execution of lines 8-14, we have $S(u) = 1$ and $S(v) = 0$. Then, by (i), used just before we have taken s from Q, we have $\psi_{\min}(\pi[u]) \geq \psi_{\min}(\pi[s])$. Thus, it is enough to show that, right after the execution of lines 8-14, we have $\psi_{\min}(\pi[s]) \geq \psi_{\min}(\pi[v])$. This clearly holds if the values $V(v)$ or $\pi[v]$ were not changed. So, assume that that have been changed. Then, as before, we see that

$$\psi_{\min}(\pi[s]) \geq \min\{\psi_{\min}(\pi[s]), w_{L(s)}(s, v)\} = \psi_{\min}(\pi[v])$$

finishing the proof of preservation of (i) and of the theorem.

5 The Local Band Constraint

Let $C\colon \mathcal{N} \to [0, \infty)$ be a fixed vertex cost function associated with an image digraph $G = \langle \mathcal{N}, \mathcal{A} \rangle$. Usually $C(t)$ is defined as a minimum of all possible path cost functions for the paths from $\mathcal{S}_1$ to t. The path cost can be its geodesic length (i.e., $\psi_{sum}(\langle v_0, \ldots, v_\ell \rangle) := \sum_{1 \leq j \leq \ell} \|v_{j-1} - v_j\|$), as used in Geodesic Star Convexity, but other path costs are also useful. It can also be based on templates of shapes discussed in [3], which will be considered for evaluation in Section 6.

The goal of this section is to construct an extension of an edge weighted digraph $G = \langle \mathcal{N}, \mathcal{A}, \omega \rangle$, discussed above to the edge weighted digraph $G' = (\mathcal{N}, \mathcal{A}', \omega')$ so that the application of OIFT (Algorithm 1) to G' produces an optimized object satisfying the Local Band constraint defined below.

To relate Local Band constraint to Boundary Band constraint introduced in [11], we first introduce the following notion of *Local Boundary Band constraint,* LBB. In this definition the symbol $\|\cdot\|$ denotes the standard Euclidean L_2 norm on $\mathcal{N} \subset \mathbb{Z}^2$. The *boundary* of an object $\mathcal{O}$ is defined as

$$\text{bd}(\mathcal{O}) = \{t \in \mathcal{O}\colon \exists s \in \mathcal{A}(t) \text{ such that } s \notin \mathcal{O}\}.$$

Definition 1 (Local Boundary Band (LBB)) *For $\Delta, R > 0$ and a cost map $C\colon \mathcal{N} \to [0,\infty)$, a pixel $t \in \mathcal{O}$ is LBB^R_Δ (satisfies Local Boundary Band Constraint with band size Δ and parameter R) provided $C(t) < C(s) + \Delta$ for all $s \in \mathrm{bd}(\mathcal{O})$ such that $\|s - t\| \leq R$. An object $\mathcal{O}$ is LBB^R_Δ provided every $t \in \mathcal{O}$ is LBB^R_Δ.*

Definition 2 (Boundary Band constraint (BB)) *For $\Delta > 0$, an object $\mathcal{O}$ is BB_Δ (satisfies Boundary Band constraint with band size Δ) provided it is $\mathrm{LBB}^\infty_\Delta$, that is, when $C(t) < C(s) + \Delta$ for all $t \in \mathcal{O}$ and $s \in \mathrm{bd}(\mathcal{O})$. As a consequence, $\mathrm{bd}(\mathcal{O})$ is contained in the band $\{s \in \mathcal{N}\colon C(s) \in (m - \Delta, m]\}$, where $m = \max\{C(t)\colon t \in \mathcal{O}\}$. In particular, $|C(s) - C(t)| < \Delta$ for all $s, t \in \mathrm{bd}(\mathcal{O})$. Consequently, this regularizes the shape of $\mathrm{bd}(\mathcal{O})$, see [11].*

The idea of BB is to establish a maximum possible variation of the cost C between the boundary points $\mathrm{bd}(\mathcal{O})$ of the object $\mathcal{O}$ to be segmented. This is expected to prevent the generated segmentation to be irregular in relation to the C-level sets [11]. During the OIFT computation subject to BB, the band changes its reference level set, allowing a better adaptation to the image content, while its width is kept fixed (Figure 1). Note that this bears some resemblance to narrow band level set [29] and to the regional context of a level line used in [30].

In BB, however, local changes in a part of the object can generate constraint violations in any other part of its boundary, usually resulting in greater sensitivity to the initialization of the cost map C and to the positioning of internal seeds, while in LBB its consistency checks are limited locally, leading to a more flexible solution. Clearly, every BB_Δ object is LBB^R_Δ, but the converse is not true. Nevertheless, for every C and Δ, there exists an $R \in (0,\infty)$ such that the property LBB^R_Δ implies BB_Δ (this certainly holds for any $R \geq \max\{\|s - t\|\colon s, t \in \mathcal{N}\}$). Thus, BB_Δ can be considered as a limit, as $R \to \infty$, of LBB^R_Δ.

In order to facilitate the implementation, we consider an approximate alternative definition, named the *Local Band constraint* (LB), in order to avoid the continuous analysis of the dynamic set of boundary pixels inside the disks of radius R at runtime, but keeping the main idea of locally restricting the band effects. This effort resulted in the following similar definition.

Definition 3 (Local Band constraint (LB)) *For $\Delta, R > 0$ and a cost map $C\colon \mathcal{N} \to [0,\infty)$, a pixel $t \in \mathcal{O}$ is LB^R_Δ (satisfies Local Band constraint with band size Δ and parameter R) provided $C(t) < C(s) + \Delta$ for all $s \in \mathcal{N} \setminus \mathcal{O}$ such that $\|s - t\| \leq R$. An object $\mathcal{O}$ is LB^R_Δ provided every $t \in \mathcal{O}$ is LB^R_Δ.*

In other words, if $\mathcal{O}$ is LB^R_Δ, then for any pair of pixels s and t such that $\|s - t\| \leq R$ and $C(t) - C(s) \geq \Delta$, we have that $t \in \mathcal{O}$ implies $s \in \mathcal{O}$. Note that neither of the statements "$\mathcal{O}$ is LB^R_Δ" and "$\mathcal{O}$ is LBB^R_Δ" implies the other. Nevertheless, they are closely related (Figure 2), as shown by the following result.

Proposition 4 *Let $r = \max_{\langle s,t\rangle \in \mathcal{A}} \|s - t\|$ and $\delta = \max_{\langle s,t\rangle \in \mathcal{A}} |C(t) - C(s)|$. If $\Delta, R > 0$ and $\mathcal{O}$ is LB^{R+r}_Δ, then $\mathcal{O}$ is $\mathrm{LBB}^R_{\Delta+\delta}$.*

Proof Choose a $t \in \mathcal{O}$. Then $C(t) < C(s) + \Delta$ for all $s \in \mathcal{N} \setminus \mathcal{O}$ such that $\|s - t\| \leq R + r$. We need to show that t is $\mathrm{LBB}^R_{\Delta+\delta}$, that is, that $C(t) < C(u) + \Delta + \delta$ for all $u \in \mathrm{bd}(\mathcal{O})$ such that $\|u - t\| \leq R$. So, take such u. Then, there is an $s \in \mathcal{N} \setminus \mathcal{O}$ with $\langle u, s\rangle \in \mathcal{A}$. Notice that $\|s - t\| \leq \|s - u\| + \|u - t\| \leq r + R$. Using this and the definition of δ, we get $C(t) < C(s) + \Delta \leq C(u) + \Delta + |C(s) - C(u)| \leq C(u) + \Delta + \delta$, as needed.

Since usually numbers δ and r are small, so should be the difference between the objects with properties LB^R_Δ, LB^{R+r}_Δ, $\mathrm{LBB}^R_{\Delta+\delta}$, or LBB^R_Δ and, for large R, each approximates BB_Δ.

The LB constraint can be implemented, as proposed in Algorithm 4 for OIFT, by considering a modified graph G' with the LB constraint embedded on its arcs. In general, the worst cost should be ∞ for Min-Sum optimizers (i.e., min-cut/max-flow algorithm) and $-\infty$ for Max-Min optimizers. In order to maintain a symmetric graph, we also create anti-parallel arcs with the best cutting cost (zero for Min-Sum and ∞ for Max-Min optimizers) if they do not exist (line 5 in Algorithm 4). Note that in G' the set of displacement vectors $D(s) = \{t - s : t \in \mathcal{A}'(s)\}$ varies for different positions of s, leading therefore to a translation-variant adjacency relation.

Algorithm 4 – Segmentation by OIFT subject to the LB constraint

Input:	Symmetric edge weighted image digraph $G = \langle \mathcal{N}, \mathcal{A}, \omega\rangle$, non-empty disjoint seed sets $\mathcal{S}_1$ and $\mathcal{S}_0$, cost map $C\colon \mathcal{N} \to [0,\infty)$, and parameters $R > 0$ and $\Delta > 0$.
Output:	The label map $L\colon \mathcal{N} \to \{0,1\}$.
Auxiliary:	Edge weighted digraph $G' = \langle \mathcal{N}, \mathcal{A}', \omega'\rangle$ with $\mathcal{A} \subset \mathcal{A}'$.

1. *Set $\mathcal{A}' \leftarrow \mathcal{A}$ and $\omega' \leftarrow \omega$.*
2. **For each** $\langle s,t\rangle \in \{\langle p,q\rangle \in \mathcal{N} \times \mathcal{N} : \|p - q\| \leq R \;\&\; C(p) \geq C(q) + \Delta\}$ **do**
3. | **If** $\langle s,t\rangle \notin \mathcal{A}'$ **then** *Set $\mathcal{A}' \leftarrow \mathcal{A}' \cup \{\langle s,t\rangle\}$ and define $\omega'(s,t) := -\infty$.*
4. | **Else** *Redefine $\omega'(s,t) := -\infty$.*
5. | **If** $\langle t,s\rangle \notin \mathcal{A}'$ **then** *Set $\mathcal{A}' \leftarrow \mathcal{A}' \cup \{\langle t,s\rangle\}$ and define $\omega'(t,s) := \infty$.*
6. *Compute, by Algorithm 1, $L\colon \mathcal{N} \to \{0,1\}$ for G' and*

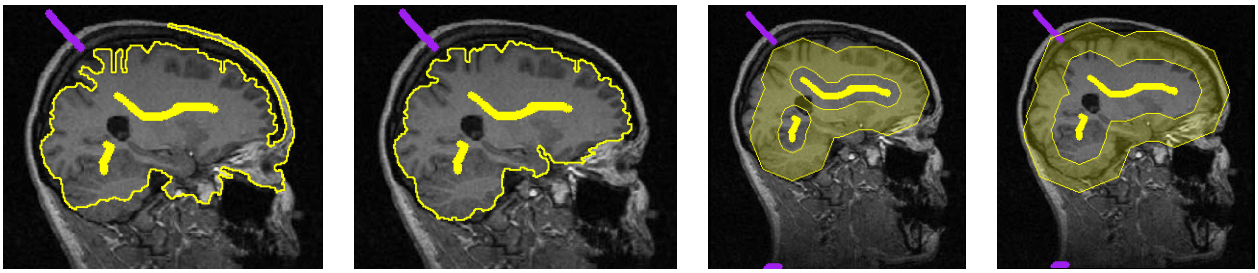

(a) (b) (c) (d)

Fig. 1 Brain segmentation example in MRI exam. (a-b) Segmentation results by OIFT without and with the BB constraint, respectively. (c-d) The BB fixed size band evolves from the seeds, adapting to the image contents. Note that the segmentation boundary achieved in (b) resides within the band area in (d).

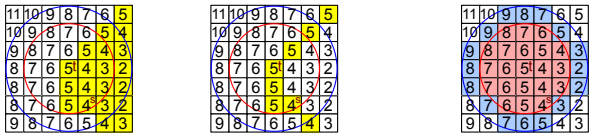

(a) $\mathcal{O}$ (yellow) (b) bd($\mathcal{O}$) (yellow) (c) Disks R and $R+r$.

Fig. 2 Example of Proposition 4, where "t is $\mathrm{LB}_{\Delta}^{R+r}$" and "$t$ is $\mathrm{LBB}_{\Delta+\delta}^{R}$" for $R = 2.5$, $r = 1.0$, $\Delta = 1$ and $\delta = 1$. (a) $\mathcal{O}$, (b) bd($\mathcal{O}$), and (c) the disks of radii R and $R+r$.

seed sets $\mathcal{S}_1$ and $\mathcal{S}_0$.

7. *Return L.*

Theorem 5 *Let $G = \langle \mathcal{N}, \mathcal{A}, \omega \rangle$ be a symmetric edge weighted image digraph with $\omega \colon \mathcal{A} \to \mathbb{R}$. Let L be a segmentation returned by Algorithm 4 applied to G, non-empty disjoint seed sets $\mathcal{S}_1$ and $\mathcal{S}_0$, cost map $C \colon \mathcal{N} \to [0, \infty)$, and parameters $R > 0$ and $\Delta > 0$. Assume that $\mathcal{S}_1$ and $\mathcal{S}_0$ are LB_{Δ}^{R}-consistent, that is, that*

($\star$) there exists a labeling satisfying seeds and LB_{Δ}^{R} constraints.

Then L satisfies seeds and LB_{Δ}^{R} constraints and maximizes the energy $\varepsilon_{\min}$, given by (1) w.r.t. G, among all segmentations satisfying these constraints.

Proof In this proof $\varepsilon_{\min}^{G}$ and $\varepsilon_{\min}^{G'}$ denote the energy $\varepsilon_{\min}$ with respect to G and G', respectively. Let $\mathcal{L} := \{\langle p, q \rangle \in \mathcal{N} \times \mathcal{N} \colon 0 < \|p - q\| \leq R \;\&\; C(p) \geq C(q) + \Delta\}$ and $\mathcal{M} := \{\langle s, t \rangle \colon (s, t) \in \mathcal{L}\} \setminus \mathcal{A}$. It is easy to see that after the execution of lines 1-5 we have $\mathcal{A}' = \mathcal{A} \cup \mathcal{L} \cup \mathcal{M}$ and

$$\omega'(s,t) = \begin{cases} -\infty & \text{for } \langle s, t \rangle \in \mathcal{L}, \\ \infty & \text{for } \langle s, t \rangle \in \mathcal{M}, \\ \omega(s,t) & \text{otherwise, that is for } \langle s, t \rangle \in \mathcal{A} \setminus \mathcal{L}. \end{cases}$$

Also, by Proposition 1, after the execution of line 6 the labeling L satisfies the seed constraints and maximizes the energy $\varepsilon_{\min}^{G'}$ among all segmentations satisfying seeds constraints. We need to show that L satisfies also LB_{Δ}^{R} constraints an that it maximizes $\varepsilon_{\min}^{G}$ among all segmentations satisfying these constraints.

To see this, let $L' \colon \mathcal{N} \to \{0, 1\}$ be an arbitrary labeling satisfying seeds and LB_{Δ}^{R} constraints. It exists by ($\star$). Then, by the definition of LB_{Δ}^{R} constraints, the set $T' := \{\langle p, q \rangle \in \mathcal{A}' \colon L'(p) > L'(q)\}$ is disjoint with $\mathcal{L}$. In particular,

$$\begin{aligned} &\varepsilon_{\min}^{G'}(L) \geq \varepsilon_{\min}^{G'}(L') \\ &= \min\{\omega'(s,t) \colon \langle s, t \rangle \in \mathcal{A}' \;\&\; L'(s) > L'(t)\} > -\infty. \end{aligned}$$

Hence

$$\varepsilon_{\min}^{G'}(L) = \min\{\omega'(s,t) \colon \langle s, t \rangle \in \mathcal{A}' \;\&\; L(s) > L(t)\} > -\infty,$$

so that the set $T := \{\langle p, q \rangle \in \mathcal{A}' \colon L(p) > L(q)\}$ must be also disjoint with $\mathcal{L}$. This means that L satisfies LB_{Δ}^{R} constraints. To finish the proof we need to show that $\varepsilon_{\min}^{G}(L) \geq \varepsilon_{\min}^{G}(L')$. For this notice first that

$$\varepsilon_{\min}^{G'}(L') = \varepsilon_{\min}^{G}(L'). \tag{2}$$

Indeed, $T' \cup T$ is disjoint with $\mathcal{L}$, so $\langle s, t \rangle \in \mathcal{A}' \;\&\; L'(s) > L'(t)$ implies that $\langle s, t \rangle \in (\mathcal{A} \setminus \mathcal{L}) \cup \mathcal{M}$. Thus, since $\omega' = \omega$ on $\mathcal{A} \setminus \mathcal{L}$ and $\omega' = \infty$ on $\mathcal{M}$,

$$\begin{aligned} \varepsilon_{\min}^{G'}(L') &= \min\{\omega'(s,t) \colon \langle s, t \rangle \in \mathcal{A}' \;\&\; L'(s) > L'(t)\} \\ &= \min\left(\{\omega'(s,t) \colon \langle s, t \rangle \in \mathcal{A} \setminus \mathcal{L} \;\&\; L'(s) > L'(t)\} \cup \{\infty\}\right) \\ &= \min\left(\{\omega(s,t) \colon \langle s, t \rangle \in \mathcal{A} \;\&\; L'(s) > L'(t)\} \cup \{\infty\}\right) \\ &= \varepsilon_{\min}^{G}(L'), \end{aligned}$$

as needed. Finally, using (2) for L and L', we obtain

$$\varepsilon_{\min}^{G}(L) = \varepsilon_{\min}^{G'}(L) \geq \varepsilon_{\min}^{G'}(L') = \varepsilon_{\min}^{G}(L'),$$

finishing the proof.

6 Experimental results

In this section we compare LB with shape constraints commonly employed in graph-based segmentation: Geodesic Star Convexity [17], Boundary Band [11], and Hedgehog Shape Prior [19,18]. We opted to compare them using Max-Min optimizers, because BB is not yet supported by Min-Sum optimizers [11].

From the IFT [13] perspective, when the cost map C is the geodesic length (i.e., $\psi_{sum}(\langle v_0, \ldots, v_\ell \rangle) := \sum_{1 \leq j \leq \ell} \|v_{j-1} - v_j\|$), from $\mathcal{S}_1$ in $G = (\mathcal{N}, \mathcal{A})$, the previous constraints are based on different attributes of a previously computed minimal forest in G rooted at $\mathcal{S}_1$: Geodesic Star Convexity uses the predecessor map [27], BB and LB constraints exploit the cost map directly, and Hedgehog uses the gradient of the cost map as vector field.

Figure 3 shows the segmentation results by OIFT using different methods, $\omega(s,t) = \|\mathcal{I}(t) - \mathcal{I}(s)\|$ and a circle template, as reference cost map, centered on the center of mass of the internal seeds. The BB constraint fails to give good results compared to Local Band, due to its greater sensitivity to the template positioning. Figure 4 shows some results of a tile segmentation using a square template and $\omega(s,t) = \|\mathcal{I}(t) - \mathcal{I}(s)\|$. In order to measure the sensitivity of the most promising methods for different seed positioning, in Figure 5 we show the accuracy curves using internal seeds in a circular brush of radius 5 pixels with horizontal displacements relative to the object's center and background seeds at the image frame. Note that, for the coin segmentation, LB ($R = 3.5$ and $\Delta = 2$) had slightly more stable results compared to Hedgehog, giving almost perfect results for 68.2% of the maximum possible horizontal shift in the coin (radius 44 pixels). BB constraint with $\Delta = 10$ had significantly lower robustness to seed displacements (11.4% of the maximum shift). For higher delta values, BB became unstable. It surprisingly had better results for a left shifted position to avoid false positives on its right side. For the wall tile segmentation, LB ($R = 3.5$ and $\Delta = 2$) had the most accurate results, giving good results for 10.3% of the maximum possible horizontal shift in the wall tile (radius 145 pixels). BB constraint with $\Delta = 10$ had worse robustness to seed displacements. For higher values of delta, it was possible to increase its robustness, but at the price of sacrificing its accuracy.

We also tested the robustness of the methods in relation to different image resolutions by quantitative experiments, to segment archaeological fragments in seven different resolutions with the geodesic cost. In order to make the experiment more challenging, the simple arc weight $\omega(s,t) = G(s) + G(t)$ was used, disregarding any prior color information, where $G(t)$ denotes the magnitude of Sobel gradient, such that we have several false boundaries (Figure 6). Figure 7 shows the mean values of the Dice coefficient for segmenting ten fragments for each image resolution, totalizing 70 executions for each method. The overall best results were obtained by LB using $R = 3.5$ and $\Delta = 2$. Hedgehog for different θ values and the same radius presented unstable results (Figure 6d). Further increasing its radius is not recommended, since it drastically increases the computational cost.

Finally, we conducted experiments with the geodesic cost to segment the liver in medical images of 40 slices of thoracic CT studies of size 512×512, using regular weights $\omega(s,t) = \|\mathcal{I}(t) - \mathcal{I}(s)\|$ and seed sets progressively obtained by eroding the ground truth and its background with twice the radius size (Figure 8). Although this scenario is apparently advantageous for the BB constraint, in view of the well-distributed and centralized seeds, LB ($R = 3.5$ and $\Delta = 2$) demonstrated good results with the highest accuracy for a large part of the curve (Figure 9a). We repeated the experiments, but now with the internal seeds shifted by 5 pixels to the left (25% of the maximum possible displacement in the central part of the curves) whenever possible. In this new scenario, the results clearly show that LB is more robust than BB in relation to seed positioning (Figure 9b).

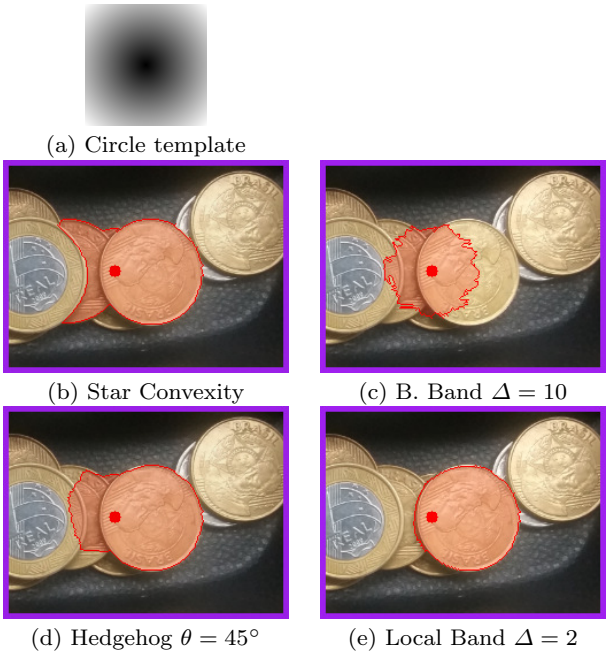

(a) Circle template

(b) Star Convexity (c) B. Band $\Delta = 10$

(d) Hedgehog $\theta = 45°$ (e) Local Band $\Delta = 2$

Fig. 3 Coin segmentation by OIFT with a circle template in a 250×185 image.

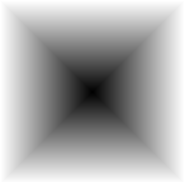

(a) Square template

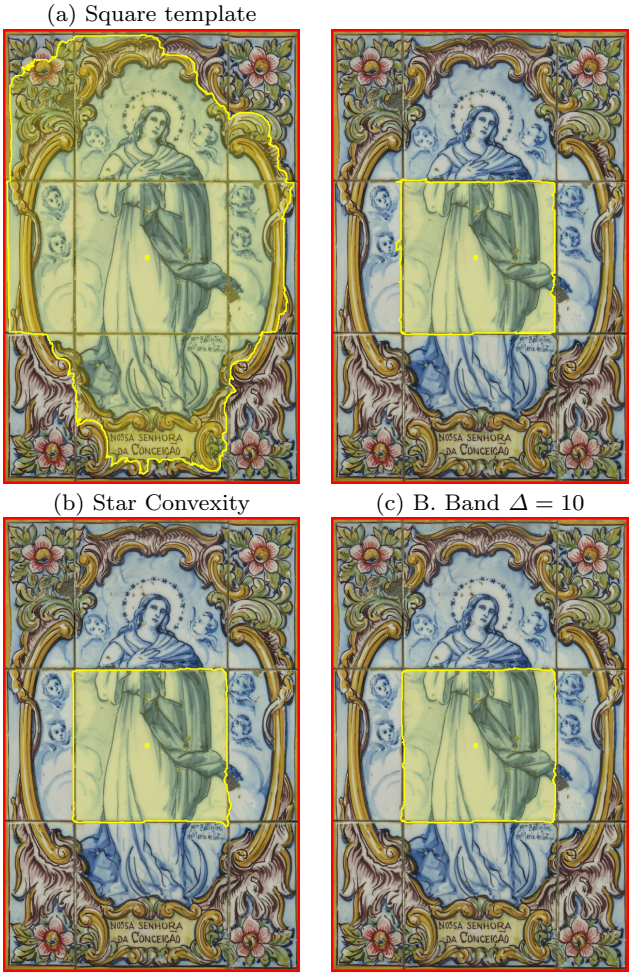

(b) Star Convexity (c) B. Band $\Delta = 10$

(d) Hedgehog $\theta = 45°$ (e) Local Band $\Delta = 2$

Fig. 4 Wall tile segmentation by OIFT with a square template in a 576×881 image.

7 Conclusion

We have proposed the Local Band shape constraint, which in its limit case (i.e., $R \to \infty$) is strongly related to Boundary Band constraint and is less sensitive to the seed/template positioning for high accuracy values. We also demonstrated that OIFT lies in the intersection of the Generalized Graph Cut and the General Fuzzy Connectedness frameworks, inheriting their properties. To the best of our knowledge, we are also the first to report OIFT with the Hedgehog shape prior. As future work, we intend to test LB in 3D medical applications.

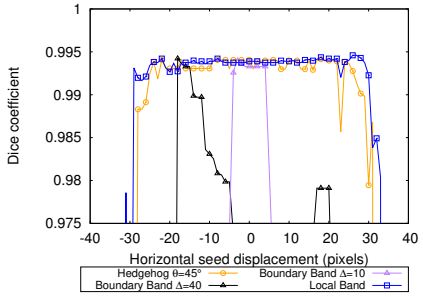

(a) coin

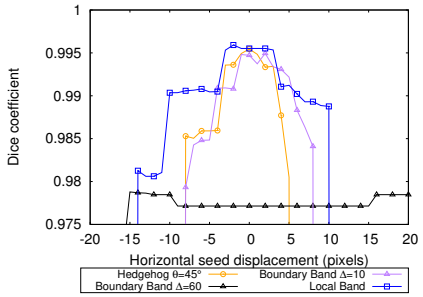

(b) wall tile

Fig. 5 The accuracy curves for different horizontal displacements of the internal seeds.

Conflict of interest

The authors declare that they have no conflict of interest.

References

1. Hans H.C. Bejar and Paulo A.V. Miranda. Oriented relative fuzzy connectedness: Theory, algorithms, and its applications in hybrid image segmentation methods. *EURASIP Journal on Image and Video Processing*, 2015(21), Jul 2015.
2. Y. Boykov and G. Funka-Lea. Graph cuts and efficient N-D image segmentation. *Intl. Jrnl. of Comp. Vision*, 70(2):109–131, 2006.
3. Caio de Moraes Braz. Segmentação de imagens pela transformada imagem-floresta com faixa de restrição geodésica. Master's thesis, Instituto de Matemática e Estatística, Universidade de São Paulo, São Paulo, Brasil, 2016.
4. K.C. Ciesielski, J.K. Udupa, A.X. Falcão, and P.A.V. Miranda. Fuzzy connectedness image segmentation in graph cut formulation: A linear-time algorithm and a comparative analysis. *Journal of Mathematical Imaging and Vision*, 44(3):375–398, Nov 2012.
5. K.C. Ciesielski, J.K. Udupa, A.X. Falcão, and P.A.V. Miranda. A unifying graph-cut image segmentation framework: algorithms it encompasses and equivalences among them. In *Proc. of SPIE on Medical Imaging: Image Processing*, volume 8314, 2012.
6. K.C. Ciesielski, J.K. Udupa, P.K. Saha, and Y. Zhuge. Iterative relative fuzzy connectedness for multiple objects with multiple seeds. *Computer Vision and Image Understanding*, 107(3):160–182, 2007.

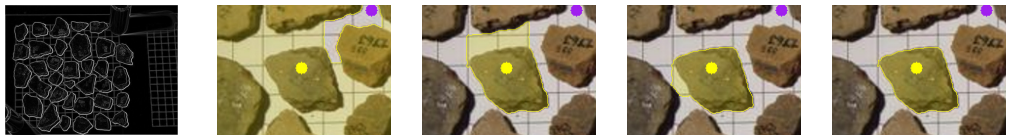

(a) Sobel gradient (b) No priors (c) B. Band (d) Hedgehog (e) Local Band

Fig. 6 Archaeological fragment segmentation.

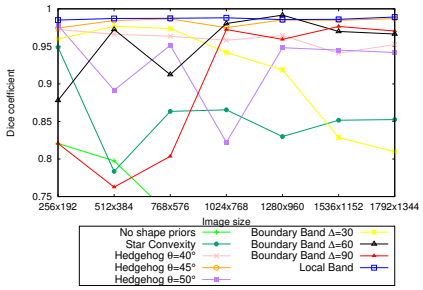

(a)

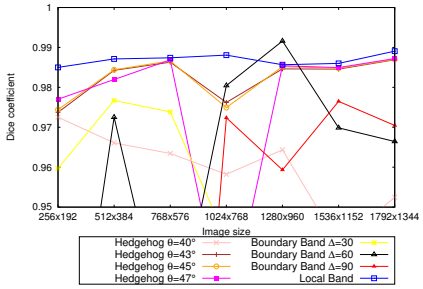

(b)

Fig. 7 (a) The mean accuracy values to segment the archaeological fragments for different image resolutions. (b) Zoomed results (accuracy $\geq 95\%$).

7. Krzysztof Chris Ciesielski, Alexandre Xavier Falcão, and Paulo A. V. Miranda. Path-value functions for which dijkstra's algorithm returns optimal mapping. *Journal of Mathematical Imaging and Vision*, 60(7):1025–1036, Sep 2018.
8. Krzysztof Chris Ciesielski, Gabor T. Herman, and T. Yung Kong. General theory of fuzzy connectedness segmentations. *Journal of Mathematical Imaging and Vision*, 55(3):304–342, Jul 2016.
9. Krzysztof Chris Ciesielski, Robin Strand, Filip Malmberg, and Punam K. Saha. Efficient algorithm for finding the exact minimum barrier distance. *Computer Vision and Image Understanding*, 123:53 – 64, 2014.
10. J. Cousty, G. Bertrand, L. Najman, and M. Couprie. Watershed cuts: Thinnings, shortest path forests, and topological watersheds. *Trans. on Pattern Analysis and Machine Intelligence*, 32:925–939, 2010.
11. C. de Moraes Braz and P.A.V. Miranda. Image segmentation by image foresting transform with geodesic band constraints. In *Image Processing (ICIP), 2014 IEEE International Conference on*, pages 4333–4337, Oct 2014.
12. Caio de Moraes Braz, Paulo A. V. Miranda, Krzysztof Chris Ciesielski, and Fábio A. M. Cappabianco. Graph-based segmentation with local band constraints. In Michel Couprie, Jean Cousty, Yukiko Kenmochi, and Nabil Mustafa, editors, *Discrete Geometry for Computer Imagery*, pages 155–166, Cham, 2019. Springer International Publishing.
13. A.X. Falcão, J. Stolfi, and R.A. Lotufo. The image foresting transform: Theory, algorithms, and applications. *IEEE TPAMI*, 26(1):19–29, 2004.
14. A.X. Falcão, J.K. Udupa, S. Samarasekera, S. Sharma, B.E. Hirsch, and R.A. Lotufo. User-steered image segmentation paradigms: Live-wire and live-lane. *Graph. Models and Image Proc.*, 60:233–260, 1998.
15. Daniel Freedman and Tao Zhang. Interactive graph cut based segmentation with shape priors. In *Computer Vision and Pattern Recognition, 2005. CVPR 2005. IEEE Computer Society Conference on*, volume 1, pages 755–762. IEEE, 2005.
16. L. Grady. Random walks for image segmentation. *IEEE Trans. Pattern Anaysis and Machine Intelligence*, 28(11):1768–1783, 2006.
17. V. Gulshan, C. Rother, A. Criminisi, A. Blake, and A. Zisserman. Geodesic star convexity for interactive image segmentation. In *Proc. of Computer Vision and Pattern Recognition*, pages 3129–3136, 2010.
18. H. Isack, O. Veksler, M. Sonka, and Y. Boykov. Hedgehog shape priors for multi-object segmentation. In *2016 IEEE Conference on Computer Vision and Pattern Recognition (CVPR)*, pages 2434–2442, June 2016.
19. Hossam N. Isack, Yuri Boykov, and Olga Veksler. A-expansion for multiple "hedgehog" shapes. *CoRR*, abs/1602.01006, 2016.
20. L. M. C. Leon and P. A. V. D. Miranda. Multi-object segmentation by hierarchical layered oriented image foresting transform. In *2017 30th SIBGRAPI Conference on Graphics, Patterns and Images (SIBGRAPI)*, pages 79–86, Oct 2017.
21. O. Lézoray and L. Grady. *Image Processing and Analysis with Graphs: Theory and Practice*. CRC Press, California, USA, 2012.
22. Xiaoqiang Li, Jingsong Chen, and Huafu Fan. Interactive image segmentation based on grow cut of two scale graphs. In Wenjun Zhang, Xiaokang Yang, Zhixiang Xu, Ping An, Qizhen Liu, and Yue Lu, editors, *Advances on Digital Television and Wireless Multimedia Communications*, pages 90–95, Berlin, Heidelberg, 2012. Springer Berlin Heidelberg.
23. A. Madabhushi and J.K. Udupa. Interplay between intensity standardization and inhomogeneity correction in MR image processing. *IEEE Transactions on Medical Imaging*, 24(5):561–576, 2005.
24. L. A. C. Mansilla and P. A. V. Miranda. Oriented image foresting transform segmentation: Connectivity constraints with adjustable width. In *29th SIBGRAPI Conference on Graphics, Patterns and Images*, pages 289–296, Oct 2016.
25. L. A. C. Mansilla, P. A. V. Miranda, and F. A. M. Cappabianco. Oriented image foresting transform segmentation with connectivity constraints. In *2016 IEEE Inter-*

(a) Seed sets (b) B. Band (c) Local Band

Fig. 8 A thoracic CT image of 512×512 pixels. (a) Seed sets obtained by eroding the ground truth of the liver (in yellow) and its background with twice the radius size (in red). (b-c) Liver segmentation samples by OIFT subject to different shape constraints.

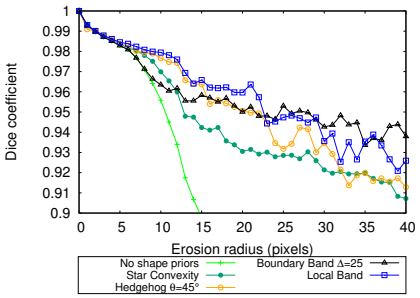

(a) $\mathcal{S}_1$ centralized

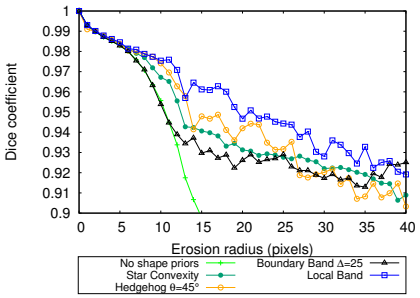

(b) $\mathcal{S}_1$ shifted to the left

Fig. 9 The mean accuracy curves to segment the liver for seed sets obtained by erosion.

national Conference on Image Processing (ICIP), pages 2554–2558, Sept 2016.

26. L.A.C. Mansilla and P.A.V. Miranda. Image segmentation by oriented image foresting transform: Handling ties and colored images. In *18th Intl. Conf. on Digital Signal Processing*, pages 1–6, Greece, Jul 2013.
27. L.A.C. Mansilla and P.A.V. Miranda. Image segmentation by oriented image foresting transform with geodesic star convexity. In *15th Intl. Conference on Computer Analysis of Images and Patterns (CAIP)*, volume 8047, pages 572–579, York, UK, Aug 2013.
28. P.A.V. Miranda and L.A.C. Mansilla. Oriented image foresting transform segmentation by seed competition. *IEEE Transactions on Image Processing*, 23(1):389–398, Jan 2014.
29. J.A. Sethian. A fast marching level set method for monotonically advancing fronts. *Proceedings of the National Academy of Sciences of the USA*, 93(4):1591–5, 1996.
30. Y. Xu, T. Géraud, and L. Najman. Context-based energy estimator: Application to object segmentation on the tree of shapes. In *2012 19th IEEE International Conference on Image Processing*, pages 1577–1580, Sept 2012.